Geophysical Research Letters

Supporting Information for

Source characteristics and along-strike variations of shallow very low frequency earthquake swarms along the Nankai Trough

Shunsuke TAKEMURA[1], Satoru BABA[1], Suguru YABE[2], Kentaro EMOTO[3], Katsuhiko SHIOMI[4], and Takanori MATSUZAWA[4]

[1]Earthquake Research Institute, the University of Tokyo, 1-1-1 Yayoi, Bunkyo-ku, Tokyo 113-0032, Japan

[2]Geological Survey of Japan, National Institute of Advanced Industrial Science and Technology, Tsukuba Central 7, 1-1-1 Higashi, Tsukuba, Ibaraki 305-8567, Japan

[3]Geophysics, Graduate School of Science, Tohoku University, 6-3, Aramaki-aza-aoba, Aoba-ku, Sendai 980-8578, Japan

[4]National Research Institute for Earth Science and Disaster Resilience, 3-1 Tennodai, Tsukuba, Ibaraki 305-0006, Japan

Contents of this file

Additional Supporting Information (Files uploaded separately)

Introduction

The methods for the detection and moment rate function estimation are described in Text S1. Figure S1 shows an example of the resultant moment rate function for a shallow VLFE. Figures S2 and S3 are comparative plots of the

estimated moment rate functions and filtered velocity envelopes with frequencies of 2–8 Hz. Spatiotemporal variations of shallow VLFEs in the A-1, A-2, and A-3 swarms are illustrated in Figure S4. Particularly, the A-1 swarm is considered to be the triggered by the Mw 7.4 intra-slab earthquake. The source characteristics of the shallow VLFE swarms are listed in Table S1. Table S2 shows the comparisons between the shallow SSEs and the corresponding swarms.

Text S1.

To detect the shallow very low frequency earthquakes (VLFEs), we calculated the cross-correlation coefficients (CCs) between the filtered template and observed seismograms every 1 s. We employed the 2nd order zero-phase Butterworth filter in the frequency range of 0.02–0.05 Hz. The blue focal spheres in Figure 1 show the template events of the shallow VLFEs. Template waveforms can be downloaded from Takemura, Noda, et al. (2019). Assuming 3.8 km/s as the propagation velocity of surface wave, the CCs at the stations were back-propagated to possible shallow VLFE epicenters, which were uniformly distributed at an interval of 0.025° on the plate boundary. We detected the events with station-averaged CCs $\geq$ 0.45 as shallow VLFE candidates. To avoid regular earthquakes and duplicate detections, we removed the local regular earthquakes listed in the unified hypocenter catalog of the Japan Meteorological Agency. We selected a shallow VLFE candidate with a maximum CC every 60 s.

We estimated the moment rate functions of the detected shallow VLFEs using a Monte Carlo-based simulated annealing technique. An open-source seismic wave propagation code (OpenSWPC; Maeda et al., 2017) was used for the calculation of the Green's function. The simulation model covered an area of 360 × 480 × 80 km^3 (black rectangle in Figure 1), discretized by grid intervals of 0.2 km in the horizontal direction and 0.1 km in the vertical direction. The 3D velocity model was constructed by combining the Japan Integrated Velocity Structure Model (JIVSM Koketsu et al., 2012) and 1D velocity models beneath the DONET stations (https://doi.org/10.5281/zenodo.4158946 Tonegawa et al., 2017). The detailed model construction process is described in Takemura et al. (2020). The possible source grids were distributed at an interval of 0.025°.

The moment rate function was estimated as follows: The epicenters and depths were fixed as relocation results and the depth of the upper surface of the Philippine Sea Plate. Previous studies have revealed that shallow VLFEs can be modeled as low-angle thrust faults on the plate boundary (e.g., Sugioka et al., 2012; Takemura et al., 2018). Thus, focal mechanisms were assumed to be low-angle thrust faults constructed by the plate geometry of JIVSM and the convergence directions of NUVEL-1A (DeMets et al., 2010). The moment rate function was constructed using a series of Küpper wavelets with a duration of 6 s. The synthetic velocity waveform $v_{ij}(t)$ from the j-th source grid to the i-th station can be written as follows:

$$v_{ij}(t) = A_0 \sum_{k=0}^{N_P-1} w_k^2 G_{ij}(t - k\Delta t)$$

where G_{ij} is the Green's function of the j-th source with a 6-s Küpper wavelet, w_k^2 is the weight of the k-th Küpper wavelet, and Δt is the offset of each pulse (3 s). Non-negative conditions (w_k^2) were imposed in our estimation. A_0 is the optimal relative amplitude

estimated by fitting the observed waveforms to synthetic waveforms based on variance reduction (e.g., Yabe et al., 2021). Using the observed waveform and amplitude-adjusted model seismogram v^{syn}, the objective function used in this analysis is as follows:

$$E = \sum_i \sum_l \left| v_{ij}^{obs}(t_l + \tau) - v_{ij}^{syn}(t_l) \right|$$

where τ is the delay time and the length of the time window is 200 s (t_l = 0–200 s). The parameters w_k^2 and τ were estimated using a Monte Carlo-based simulated annealing procedure. Δw = 0.02 and $\Delta\tau$ = 0.5 s were perturbed at each time step for the source weights (w_k) and delay time (τ), respectively. According to shallow VLFE duration measurements derived from offshore broadband analysis (Sugioka et al., 2012), the number of source weight parameters was 40; thus, the maximum duration of the modeled moment rate function was 123 s.

The initial temperature and cooling rate in the simulated annealing were T_0 = $3E_0$ and γ = 0.996, respectively (e.g., Tocheport et al., 2007). We initially assumed w_k^2 = 1, which was not able to reproduce the observed seismograms (Figure 2b). $T_k = \gamma^k T_0$ gives the annealing schedule at the k-th iteration. The perturbation at the k-th iteration with ΔE_k (= E_k-E_{k-1}) < 0 was fully accepted. We also accepted the perturbation with $\Delta E_k \geq 0$ and the probability of $P = \exp(-\Delta E_k/T_k)$ equal to less than α, which is a random number between 0 and 1 at each iteration.

The estimations were conducted using a frequency band of 0.02–0.05 Hz to avoid the effects of microseisms at onshore stations (e.g., Nishida, 2017). In some cases, the resultant moment rate functions have longer-duration late moment releases, which do not contribute to the reproducibility of observed shallow VLFE signals with frequencies of 0.02–0.05 Hz (e.g., Figure 2 of Takemura et al., 2021). Due to such band-limited analysis, we could not distinguish whether the longer-duration late moment release in the simulated annealing result was a source energy release or an artifact (Figure S3 of Takemura et al., 2021). Additionally, our method might model the reverberations of later weak surface waves within the oceanic sediments and noise signals as a seismic moment release from the source for cases with a low signal-to-noise ratio. Therefore, to avoid misestimating the moment rate functions after simulated annealing, especially due to noise signals, we calculated the variance reductions (VRs) between the observed and synthetic seismograms that were constructed using N Küpper pulses. We adopted the N-th (N = 1–40) parameters, which achieved 90% of the maximum VR (VR_m) for simulated annealing. Several thresholds were tested in a previous study (Takemura et al., 2021).

After obtaining the optimal solution, we calculated the VR values between the observed and optimal syntenic seismograms. These VR values represented the goodness-of-fit factors for the optimal solutions. For shallow VLFEs with lower VRs (<30%), the signals at onshore F-net stations could be weak compared to the noise signals; consequently, their durations might be misestimated due to low signal-to-noise ratio

conditions. Therefore, in subsequent discussions of shallow VLFE activities, we discarded the results with VRs <30%.

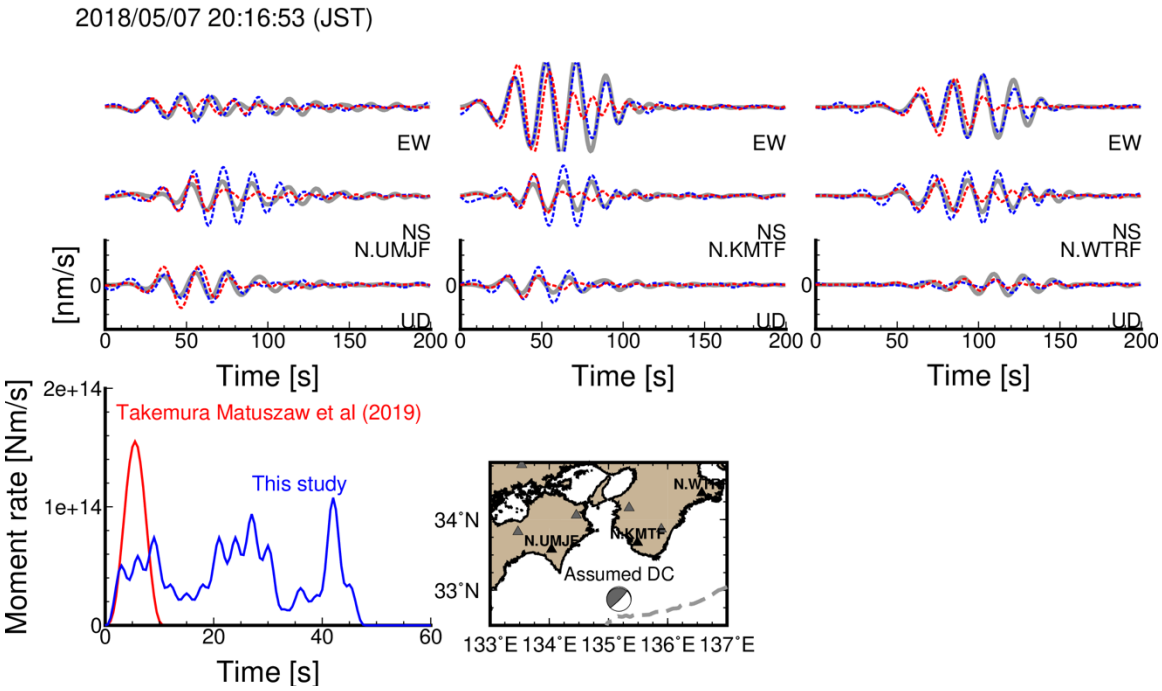

Figure S1. Comparison of estimated moment rate functions between this study (blue lines) and a previous study (red lines, Takemura, Matsuzawa, et al., 2019). In the upper panel, gray, red, and blue lines represent the observed waveforms, synthetic waveforms of Takemura, Matsuzawa, et al. (2019), and synthetic waveforms of this study, respectively. A band-pass filter of 0.02–0.05 Hz was applied. Station locations are shown on the map. Estimated moment rate functions are illustrated in the left bottom panel. Estimated seismic moments of Takemura, Matsuzawa, et al. (2019) and this study are 7.24×10^{14} and 2.04×10^{15} Nm, respectively.

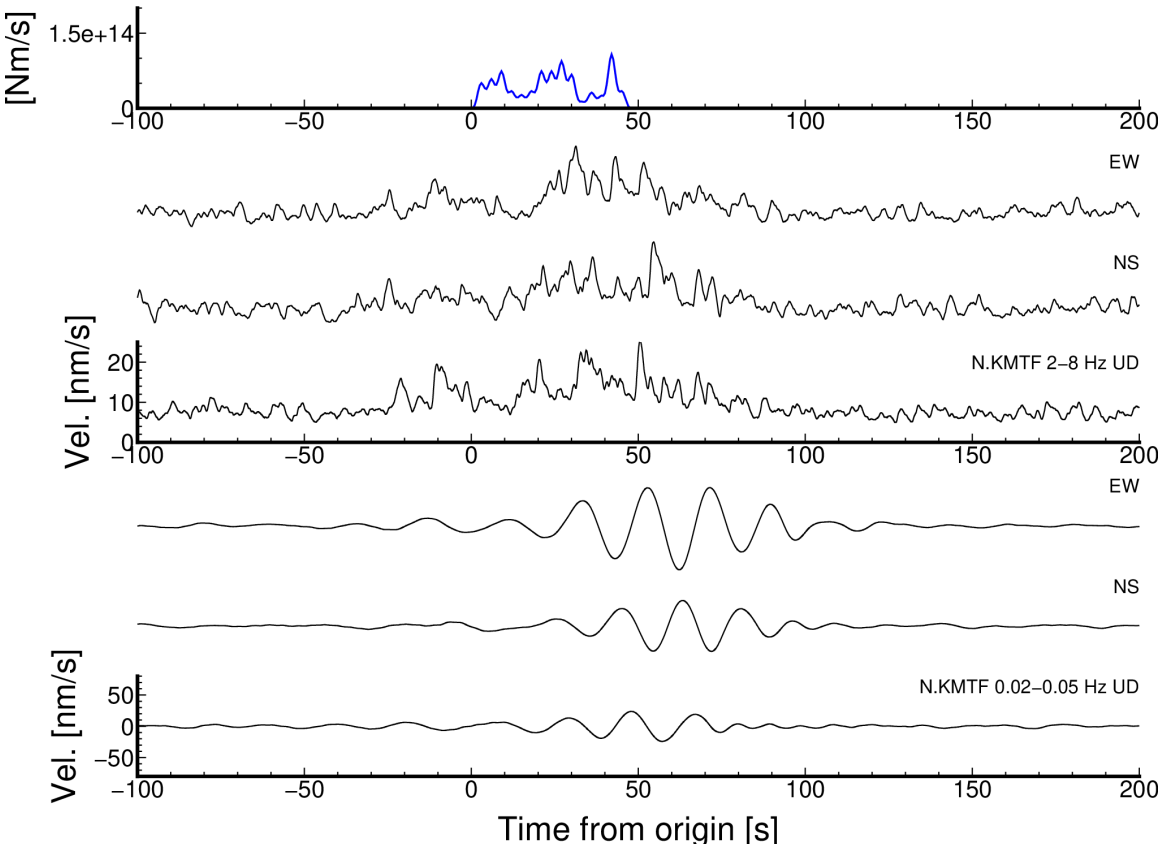

Figure S2. Comparison of low-frequency waveforms and high-frequency envelopes at N.KMTF during a shallow VLFE occurred at 20:16:53 on May 7, 2018 (JST). We also plotted the estimated moment rate function of a shallow VLFE (blue line) in the upper panel.

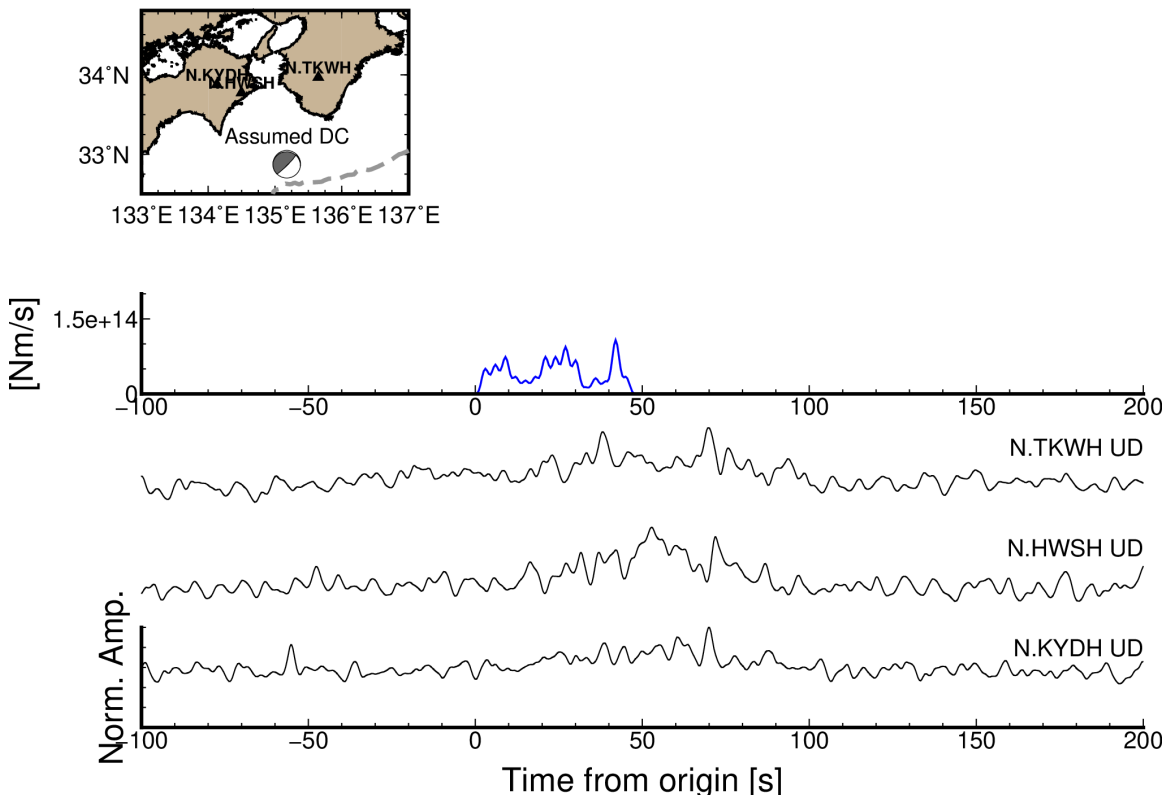

Figure S3. Examples of high-frequency (2–8 Hz) envelopes of vertical velocity seismograms at Hi-net (National Research Institute for Earth Science and Disaster Resilience, 2019) stations during a shallow VLFE that occurred at 20:16:53 on May 7, 2018 (JST). We also plotted the estimated moment rate function of a shallow VLFE (blue line) in the upper panel. Locations of used Hi-net stations are shown in the map.

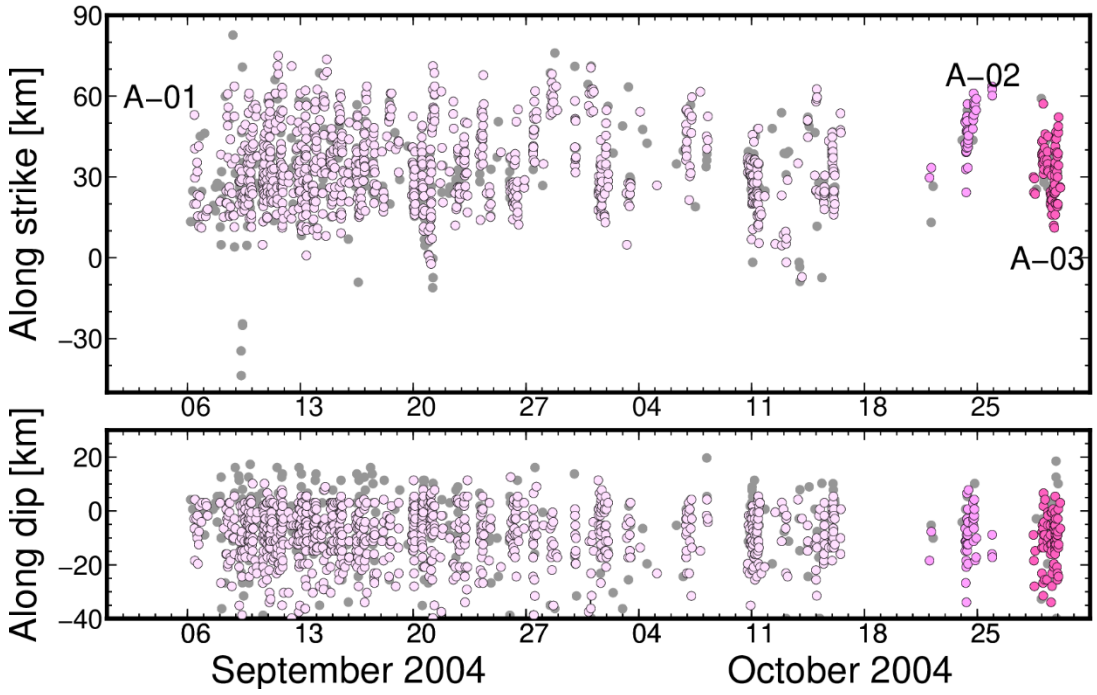

Figure S4. Spatiotemporal variations of shallow VLFEs during swarms A-01, 02, and 03. Gray circles indicate the shallow VLFEs with VR <30%.

Table S1. List of the detected shallow VLFE swarms in this study. Durations of the swarms are times between the initial and final shallow VLFEs in each swarm. The areas and cumulative moments were evaluated using shallow VLFEs with VRs equal to or greater than 30%.

Index	Initial date (JST)	Duration [s]	Areas [m^2]	Along-strike dist. [m]	Cum. Moment [Nm]
A-01	2004-09-06T04:40:12.00	3485898.0	3.59E+09	82153.8	1.38E+18
A-02	2004-10-22T00:58:02.50	336205.0	9.28E+08	39336.1	5.14E+16
A-03	2004-10-28T11:46:34.00	360075.5	1.79E+09	63303.8	8.26E+16
A-04	2004-11-13T00:07:21.00	264886.0	1.17E+09	47603.7	5.12E+16
A-05	2004-12-13T02:26:08.50	180772.0	1.18E+09	50479.7	1.17E+17
A-06	2004-12-27T02:52:39.00	328496.5	2.55E+08	19132.6	4.00E+16
A-07	2005-08-29T00:28:33.50	366288.0	9.94E+08	34807.2	9.46E+16
A-08	2007-07-21T04:13:54.00	326033.5	9.12E+08	37379.0	1.71E+16
A-09	2009-03-24T04:16:39.00	959886.5	2.78E+09	79642.1	3.11E+17
A-10	2009-04-08T21:09:14.50	347819.0	8.23E+08	32544.7	2.98E+16
A-11	2009-04-27T14:11:43.50	97245.5	1.64E+08	7415.6	1.24E+16
A-12	2016-04-03T07:01:47.00	731415.5	7.43E+08	30236.3	4.18E+16
A-13	2018-05-03T11:06:20.50	100466.0	6.13E+07	7417.1	2.38E+15
A-14	2020-12-06T21:12:18.50	1458580.0	2.68E+09	69854.3	2.92E+17
A-15	2020-12-28T12:49:51.50	153422.5	1.10E+09	42753.7	5.73E+16
A-16	2021-01-12T04:13:09.00	179378.0	5.23E+08	27757.4	1.16E+16
B-01	2004-04-29T21:53:19.00	1517602.5	3.28E+08	32067.2	1.30E+16
B-02	2008-03-23T01:07:54.00	1120895.0	1.46E+08	15425.3	5.00E+15
B-03	2016-04-06T07:12:00.00	360198.0	6.15E+07	9684.3	2.70E+15
B-04	2020-12-30T23:24:55.00	1229535.5	4.08E+08	40898.4	6.21E+15
C-01	2004-09-06T15:03:51.50	2418988.5	1.77E+09	90990.3	5.88E+16
C-02	2004-10-31T22:04:16.50	3341780.0	3.05E+08	35122.4	5.83E+15
C-03	2006-08-19T00:31:25.00	1674820.5	1.46E+08	8947.2	1.02E+16
C-04	2009-03-19T01:17:53.50	10884568.5	5.15E+09	102606.0	1.44E+17
C-05	2010-01-13T04:29:05.00	5602565.0	1.56E+09	61370.3	1.50E+16
C-06	2011-03-08T21:28:16.00	2567116.5	3.76E+09	113715.0	2.87E+16
C-07	2014-12-01T18:28:55.50	974671.0	2.02E+08	10625.4	2.35E+16
C-08	2015-08-25T16:45:28.50	2686835.0	1.91E+08	15826.8	3.00E+16
C-09	2018-02-28T08:27:26.00	7952416.0	3.12E+09	80469.0	1.35E+17

Table S2. Comparisons of seismic moments between shallow SSEs and VLFE swarms.

Period	Reg.	Mo of Shallow SSE [Nm]	Reference of shallow SSEs	Cum. Mo of shallow VLFEs [Nm]	VLFE swarms index
March 2009~ July 2009	C	2.51×10^{18}	Yokota & Ishikawa, 2020	1.44×10^{17}	C-04
April 2016	A	2.51×10^{18}	Itaba, 2018	0.46×10^{17}	A-12 and B-03
March 2018~ May 2018	C	1.00×10^{18}	Yokota & Ishikawa, 2020	1.34×10^{17}	C-09
Dec. 2020~ Jan. 2021	A	$2.5\sim10.0\times10^{18}$	Geological Survey of Japan AIST, 2021	3.67×10^{17}	A-14, 15, 16, and B-04

References of supporting information

DeMets, C., Gordon, R. G., & Argus, D. F. (2010). Geologically current plate motions. *Geophysical Journal International*, *181*(1), 1–80. https://doi.org/10.1111/j.1365-246X.2009.04491.x

Geological Survey of Japan, N. I. of A. I. S. and T., & National Research Institute for Earth Science and Disaster Resilience. (2021, September). Short-term slow slip events in the Tokai area, the Kii Peninsula and the Shikoku District, Japan (from November 2020 to April 2021). Retrieved November 8, 2021, from https://cais.gsi.go.jp/YOCHIREN/report/kaihou106/06_03.pdf

Itaba, S. (2018). *Detection of shallow SSE Off the Kii Peninsula by an onland borehole strain observation network*. Retrieved from http://www.tries.jp/research/doc/2018061416302928_22.pdf

Koketsu, K., Miyake, H., & Suzuki, H. (2012). Japan Integrated Velocity Structure Model Version 1. *Proceedings of the 15th World Conference on Earthquake Engineering*, 1–4.

Maeda, T., Takemura, S., & Furumura, T. (2017). OpenSWPC: an open-source integrated parallel simulation code for modeling seismic wave propagation in 3D heterogeneous viscoelastic media. *Earth, Planets and Space*, *69*(1), 102. https://doi.org/10.1186/s40623-017-0687-2

National Research Institute for Earth Science and Disaster Resilience. (2019). NIED Hi-net. https://doi.org/10.17598/NIED.0003

Nishida, K. (2017). Ambient seismic wave field. *Proceedings of the Japan Academy, Series B*, *93*(7), 423–448. https://doi.org/10.2183/pjab.93.026

Sugioka, H., Okamoto, T., Nakamura, T., Ishihara, Y., Ito, A., Obana, K., et al. (2012). Tsunamigenic potential of the shallow subduction plate boundary inferred from slow seismic slip. *Nature Geoscience*, *5*(6), 414–418. https://doi.org/10.1038/ngeo1466

Takemura, S., Matsuzawa, T., Kimura, T., Tonegawa, T., & Shiomi, K. (2018). Centroid Moment Tensor Inversion of Shallow Very Low Frequency Earthquakes Off the Kii Peninsula, Japan, Using a Three-Dimensional Velocity Structure Model. *Geophysical Research Letters*, *45*(13), 6450–6458. https://doi.org/10.1029/2018GL078455

Takemura, S., Noda, A., Kubota, T., Asano, Y., Matsuzawa, T., & Shiomi, K. (2019). Migrations and Clusters of Shallow Very Low Frequency Earthquakes in the Regions Surrounding Shear Stress Accumulation Peaks Along the Nankai Trough. *Geophysical Research Letters*, *46*(21), 11830–11840. https://doi.org/10.1029/2019GL084666

Takemura, S., Matsuzawa, T., Noda, A., Tonegawa, T., Asano, Y., Kimura, T., & Shiomi, K. (2019). Structural Characteristics of the Nankai Trough Shallow Plate Boundary Inferred From Shallow Very Low Frequency Earthquakes. *Geophysical Research Letters*, *46*(8), 4192–4201. https://doi.org/10.1029/2019GL082448

Takemura, S., Yabe, S., & Emoto, K. (2020). Modelling high-frequency seismograms at ocean bottom seismometers: effects of heterogeneous structures on source parameter estimation for small offshore earthquakes and shallow low-frequency tremors. *Geophysical Journal International*, *223*(3), 1708–1723. https://doi.org/10.1093/gji/ggaa404

Takemura, S., Obara, K., Shiomi, K., & Baba, S. (2021). Spatiotemporal variations of shallow very low frequency earthquake activity southeast off the Kii Peninsula, along the Nankai Trough, Japan. *ESSOAr*. https://doi.org/10.1002/essoar.10507824.1

Tocheport, A., Rivera, L., & Chevrot, S. (2007). A systematic study of source time functions and moment tensors of intermediate and deep earthquakes. *Journal of Geophysical Research: Solid Earth*, *112*(7), 1–22. https://doi.org/10.1029/2006JB004534

Tonegawa, T., Araki, E., Kimura, T., Nakamura, T., Nakano, M., & Suzuki, K. (2017). Sporadic low-velocity volumes spatially correlate with shallow very low frequency earthquake clusters. *Nature Communications*, *8*(1), 2048. https://doi.org/10.1038/s41467-017-02276-8

Yabe, S., Baba, S., Tonegawa, T., Nakano, M., & Takemura, S. (2021). Seismic energy radiation and along-strike heterogeneities of shallow tectonic tremors at the Nankai Trough and Japan Trench. *Tectonophysics*, *800*, 228714. https://doi.org/10.1016/j.tecto.2020.228714

Yokota, Y., & Ishikawa, T. (2020). Shallow slow slip events along the Nankai Trough detected by GNSS-A. *Science Advances*, *6*(3), eaay5786. https://doi.org/10.1126/sciadv.aay5786